Localisation of Skull Fracture Initiation

Karin A Rafaels, Erika A Matheis, Andrew D Brown

I. INTRODUCTION

To protect the brain, the skull can absorb energy from impact events by fracturing. Therefore, to predict head injury, it is important to correctly predict skull fracture initiation, propagation and post-fracture response. Computational models have become a useful tool to predict the tissue response from a variety of impact scenarios and develop protection solutions. However, current skull fracture models use a variety of metrics to predict fracture from correlations to head acceleration metrics [1-2] to thresholds based on stress [3], strain [4], or energy [5], with no consensus on a unified criterion. Most of these studies used documented skull fracture patterns to define and validate their specific thresholds. Further development and validation of skull fracture modeling and predictions could be achieved if the timing and location of fracture initiation could also be used. This study documents a method to calculate the approximate timing and location of fractures from impacts to the head.

II. METHODS

Acoustic emission (AE) serves as a nondestructive technique to detect bursts of activity from elastic waves generated from fracture events during mechanical testing. AE has previously been used to monitor fracture modes in human facial and long bones and vertebrae [6-8]. One of the main advantages of AE techniques is that the sensors do not need to be mounted near the fracture site and can detect defects even if loads can continue to be supported after a fracture occurs, unlike with strain gauges [6]. In this study, three AE sensors (Pico or Micromini S9225 AE, Physical Acoustics Corporation, West Windsor Township, NJ) were attached to the skulls of post-mortem human subjects (PMHS) surrounding the impact location on the same bone using cyanoacrylate adhesive, nominally 30–50 mm from the intended impact location, to triangulate the location of the fracture initiation. After instrumentation, the skin was carefully secured back in place using post-mortem staples.

An impact condition expected to generate a fracture using a compliant impactor (approximate diameter of 90 mm) was applied to the frontal bone along the midline, approximately 66 mm from bregma. Two fresh/frozen, head/neck specimens from male PMHS-donors aged 76 and 79 with approximately 50th percentile stature and mass were tested. All testing was done in accordance with the US DEVCOM Army Research Laboratory Policy for Use of Human Cadavers for Research, Development, Test, and Evaluation.

An input voltage of 28 V was supplied to a 40-dB pre-amplification signal conditioner and acoustic sensor. The data was collected at either 2 or 25MHz. The raw data was initially filtered using a fourth-order, high-pass Butterworth filter with a cutoff frequency of 150kHz. The signal was then normalised based on the maximum absolute voltage value and rectified to more easily compare the signals from the different sensors and evaluate the energy released by the fractures. To identify a potential fracture event, a threshold of 6 dB (1 mV) for a positive rise above the noise floor was selected based on increased noise levels between signal bursts post-impact. Although the actual energy released is an unknown, the relative energy release was estimated as the areas under the signal envelopes post-thresholding [8]. The timing of the potential fracture events, sensor locations, and the Rayleigh wave speed for cranial bone (1350 m/s) [9] were used to calculate the approximate location of fracture initiation. CT scans were used to measure sensor locations and skull surface distances.

III. INITIAL FINDINGS

Linear fractures that were not directly under the impact site were produced in each test (Fig 1). The fracture in the 79 yo specimen was only on the outer table, whereas the fracture in the 76 yo specimen was longer and present through the thickness of the skull. Measured AE signals from each test were able to capture differences in timing and relative energy (Fig 1). An assumption was made that the peak voltage of burst events in the AE signals is directly proportional to some combination of their nucleation distances from the AE sensors and the

K.A. Rafaels, PhD (karin.a.rafaels.civ@army.mil, 240-687-4174) is a Biomedical Engineer at the US DEVCOM Army Research Laboratory in Aberdeen Proving Ground, MD, USA. E.A. Matheis is Biomedical Engineer for SURVICE Engineering in Belcamp, MD, USA. A.D.Brown, PhD is a Mechanical Engineer at the US DEVCOM Army Research Laboratory in Research Triangle Park, NC, USA.

amount of energy released by an associated fracture. The calculated location of fracture initiation between these two tests differed despite impacts to a similar region (Fig 1) with one fracture initiating near the orbital ridge and the fracture in the other specimen initiating near the boundary of the impact area.

The time from impact to the onset of an emission signal from all of the sensors matched the wave transit time using the Rayleigh wave speed between the impact site and the sensor location. When the relative energy release rate (RERR) had a large increase, it indicated that a fracture had occurred. The timing of the jumps in the RERR between the sensors and the wave transit time using the Rayleigh wave speed was used to localize the fracture initiation. There was only one position on the skull where the fracture existed and the timings between the increase in RERR of the sensors aligned. This was determined to be the fracture initiation location. Unpublished simulations of these impacts also indicated similar timing and location of high tensile strains that exceed the 1% tensile strain tolerance level for cortical skull [10] as the fractures identified in the experiments.

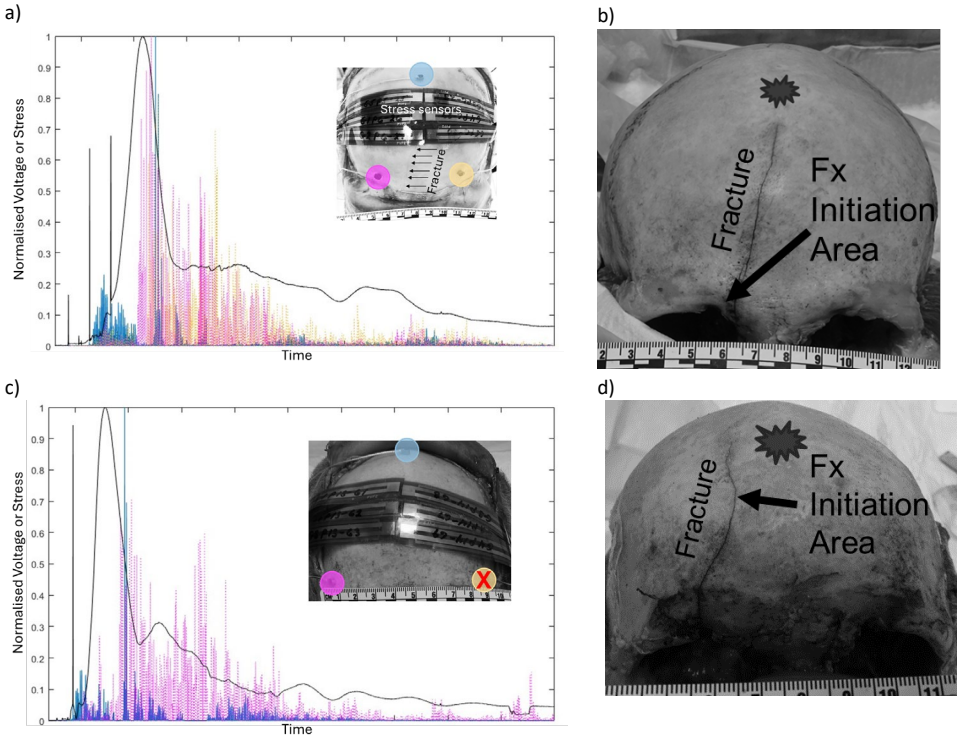

Fig 1. a) Acoustic emission sensor placement and data (76 yo) after filtering, normalisation, rectification, and thresholding. The colour of the highlighted sensor matches the colour in the AE plot. The solid black line represents the total force measured from the stress sensors under the impact site. b) Depiction of impact location (explosion symbol), fracture and calculated fracture initiation location (76 yo). c) Acoustic emission sensor placement and data (79 yo) after filtering, normalisation, rectification, and thresholding. The colour of the highlighted sensor matches the colour in the AE plot. The yellow-highlighted sensor did not produce a usable signal in this test. The solid black line represents the total force measured from the stress sensors under the impact site. d) Depiction of impact location (explosion symbol), fracture and calculated fracture initiation location (79 yo).

IV. DISCUSSION

Crack detection using time of arrival techniques has been used in various applications [11,12]; however, it is critical to use the appropriate wave speed [13]. In this study, the fractures were witnessed on the outer table, and in one case, only on the outer table. Under impact conditions where fractures begin to initiate on the skull, tensile failure on the outer surface has been identified as the mechanism [14]. Considering the nature of these surface-breaking fractures, an analysis using Rayleigh wave speeds was used, compared to other effective velocity methods [15]. Rayleigh waves can travel farther and across complex geometries and surfaces compared to bulk waves making them better suited for remote detection of fractures on the skull, particularly when there is high frequency content [16], as was the case for this impact condition.

The relative energy of the emission at each sensor location can provide insights into the propagation of the fracture. Being able to model this post-failure, fracture propagation behavior is important for predicting the severity of injuries in computational models as the extent and location have been related to injury severity [17].

V. REFERENCES

[1] Wang F *et al.*, Biomimetics, 2023. [2] Klug C *et al.*, 2023. 27th Int. ESV Conference, 2023. [3] Palomar M *et al.*, Compos Struct, 2018. [4] Lindgren N *et al.*, Biomech Model Mechan, 2023. [5] De Kegel D *et al.*, J Mech Behav Biomed Mater, 2019. [6] Cormier J, Dissertation, 2009. [7] Aggelis DG *et al.*, Sensors, 2015. [8] Goodwin BD *et al.*, Ann Biomed Eng, 2017. [9] Estrada H *et al.*, Ultrasound Med Biol, 2018. [10] Boruah *et al.*, JMBBM, 2017. [11] Nivesrangsan P *et al.*, Mech Syst Signal Process, 2007. [12] Tobias A, Non-Destr Test, 1976. [13] Kaphle *et al.*, Struct Control Health Monit, 2012. [14] Gurdjian ES *et al.*, Radiology, 1950. [15] Shridharani JK *et al.*, Proc IRCOBI Conf, 2014. [16] Achenbach JD *et al.*, Proc DARPA/AFWAL Quant NDE, 1981. [17] Chattopadhyay S *et al.*, J Inj Violence Res, 2010.